Carbohydrate Polymers 169 (2017) 108–116

Contents lists available at ScienceDirect

Carbohydrate Polymers

journal homepage: www.elsevier.com/locate/carbpol

Chemical modification of nanocellulose with canola oil fatty acid methyl ester

Liqing Wei [a], Umesh P. Agarwal [a], Kolby C. Hirth [a], Laurent M. Matuana [b], Ronald C. Sabo [a,*], Nicole M. Stark [a,*]

[a] USDA Forest Service, Forest Products Laboratory, One Gifford Pinchot Drive, Madison, WI 53726, United States
[b] School of Packaging, Michigan State University, East Lansing, MI 48824, United States

ARTICLE INFO

Article history:
Received 22 February 2017
Accepted 3 April 2017
Available online 4 April 2017

Keywords:
Nanocellulose
Transesterification
Crystallinity
Vegetable oil
Hydrophobiciy

ABSTRACT

Cellulose nanocrystals (CNCs), produced from dissolving wood pulp, were chemically functionalized by transesterification with canola oil fatty acid methyl ester (CME). CME performs as both the reaction reagent and solvent. Transesterified CNC (CNCFE) was characterized for their chemical structure, morphology, crystalline structure, thermal stability, and hydrophobicity. Analysis by Fourier transform infrared (FTIR) and FT-Raman spectroscopies showed that the long chain hydrocarbon structure was successfully grafted onto CNC surfaces. After transesterification the crystal size and crystallinity of nanocrystals were not changed as determined by Raman spectroscopy and wide angle X-ray diffraction (XRD). CNCFE showed higher thermal stability and smaller particle size than unmodified CNCs. Water contact angle measurement indicated the CNCFE surface has significantly higher hydrophobicity than unmodified CNCs. The transesterified CNCs could be potentially used as hydrophobic coatings and reinforcing agents to hydrophobic polymer for nanocomposites.

Published by Elsevier Ltd.

1. Introduction

Biobased materials are attracting immense research interest because of their low negative impact to environment at the end of service life. Cellulose nanomaterials have been known more than half century ago and have gained extraordinarily renewed attention in recent years. Generally, two forms of nanocellulose, the cellulose nanocrystals (CNCs) and cellulose nanofibrils (CNF), have been produced. CNCs exhibit impressive properties such as low-density, high mechanical strength, low thermal expansion, and excellent biocompatibility and renewability (Moon, Beck, & Rudie, 2013). The tensile modulus of CNCs can reach to 170 GPa because of its high crystallinity (54–90%) (Habibi, Lucia, & Rojas, 2010; Klemm et al., 2011; Wei & McDonald, 2016). This has shown great promise of CNCs as reinforcing agents (Bardet, Roussel, Coindeau, Belgacem, & Bras, 2015; Habibi et al., 2010; Moon et al., 2013; Pereira et al., 2014). CNCs can be produced from cellulose derived from trees, plants, tunicates, bacteria and algae. Acid hydrolysis, with sulfuric acid generally, is used to remove most amorphous fractions of cellulose to prepare CNCs (Moon et al., 2013; Reiner & Rudie, 2013). The negatively charged surfaces of CNCs result in stable colloidal suspensions of CNC in water. However, similar to general cellulose, the abundant hydroxyl groups on CNC surfaces make it a highly hydrophilic material, which often impairs its excellent properties.

In this situation, various approaches have been investigated to modify CNC and tune its surface chemistry. In some methods, CNCs are modified during the production step (Boujemaoui, Mongkhontreerat, Malmström, & Carlmark, 2015; Espino-Pérez, Domenek, Belgacem, Sillard, & Bras, 2014), while in other strategies the CNCs were produced first followed by the modifications, such as acetylation (Abraham et al., 2016; Lin, Huang, Chang, Feng, & Yu, 2011; Ramírez, Fortunati, Kenny, Torre, & Foresti, 2016) and polymer grafting (Eyley & Thielemans, 2011; Hatton, Kedzior, Cranston, & Carlmark, 2017; Morandi, Heath, & Thielemans, 2009). The main challenge with chemical functionalization to CNCs is to select an appropriate method, namely the surface modification that would not impact the distinctive properties of CNCs. For example, if the 3D crystal network is interrupted during modification the mechanical properties of CNCs could deteriorate, which could consequently limit the applications of modified CNC (Klemm, Heublein, Fink, & Bohn, 2005; Klemm et al., 2011). Those mentioned CNC modification approaches can be relatively easily achieved with the use of organic solvents or toxic reagents, such as dimethylformamide, toluene diisocyanate, and halogenated solvent. In addition, some

* Corresponding authors.
E-mail addresses: rsabo@fs.fed.us (R.C. Sabo), nstark@fs.fed.us (N.M. Stark).

http://dx.doi.org/10.1016/j.carbpol.2017.04.008
0144-8617/Published by Elsevier Ltd.

water based approaches have been used to modify CNC surfaces, for example, Zaman et al. have used glycidyltrimethylammonium chloride to modify CNC to render its cationic surfaces formed during acid hydrolysis process (Zaman, Xiao, Chibante, & Ni, 2012). Yoo and Youngblood have applied an one-pot synthesis approach to graft lactic acid onto CNC surfaces to produce a CNC-grafted-PLA copolymer (Yoo & Youngblood, 2016). However, the hydrophobicity of modified CNCs was not increased. Thus, the preparation of modified CNCs with intact properties by using "sustainable chemistry" based strategy is still challenging in nanocellulose research.

Vegetable oil, a triglyceride, is a promising renewable resource and after transesterification reaction with an alcohol (commonly methanol) the fatty acid methyl ester (FAME) is produced (Lang, Dalai, Bakhshi, Reaney, & Hertz, 2001). Most common fatty acids present in vegetable oils include palmitic (C16:0), stearic (C18:0), oleic (C18:1), linoleic (C18:2), linolenic (C18:3), and ricinoleic (C18:1, OH) acids. While the long hydrocarbon chain of the fatty acid continues to be strongly hydrophobic, the presence of the carboxylic acid group at one end of the molecule adds some hydrophilic properties to fatty acids (Yoo & Youngblood, 2016). When fatty acids are converted into FAME, the hydrophobic long chain hydrocarbon structure could be chemically bonded to CNCs by the second transesterification reaction between the hydroxyl (OH) groups and FAME. To our knowledge, this type of transesterification has not been studied for the modification of nanocellulose.

In this study, CNCs were produced by sulfuric acid hydrolysis of wood-derived dissolving pulp followed by freeze-dried process. FAME was prepared by the first transesterification reaction between canola oil and methanol, and then used to modify CNCs via the second transesterification. GC–MS was used to determine the molecular weight of FAME adducts. The chemical and crystalline structures of produced transesterified CNCs were characterized by FT-IR, FT-Raman and XRD analyses. Thermal stability was studied by thermogravimetric analysis (TGA). Surface hydrophobicity of CNCs was evaluated by water contact angle measurement. The results provide insight into an environmentally benign chemical modification of CNC to broaden its application as hydrophobic coatings and reinforcing agent for hydrophobic polymers.

2. Experimental

2.1. Materials

Cellulose nanocrystals (CNCs, 2014-FPL-CNC-065) were produced by USDA-Forest Service, Forest Products Laboratory (Madison, Wisconsin) using sulfuric acid hydrolysis method. Briefly, the prehydrolyzed kraft rayon-grade dissolving Eucalyptus dry lap wood pulp was used as the starting material for producing the CNCs. The dissolving wood pulp contains 78.1%, 15.5%, and 0.1% of cellulose, hemicellulose, and Klason lignin, respectively (Wang et al., 2012). Bundles of the dissolving pulp were reacted with 64% sulfuric acid (acid:cellulose = 8:1 (v:w)) at 45 °C for about 1.5 h under a nitrogen blanket with constant stirring. The hydrolysis was quenched by diluting the reaction mixture with distilled water to approximately a 10-fold volume of the initial mixture. The CNC were neutralized by adding a NaOH solution (5 wt%). The sodium sulfate and other salts were removed by ultrafiltration to retain the CNC concentration at approximately 1%. After all salts are removed, the CNC suspension was concentrated to have 10.7 wt% of solid (Reiner & Rudie, 2013). The liquid CNC suspension (10.7 wt%) was freeze-dried to obtain dry CNCs materials. The sulfur content of CNCs was analyzed using an ICP-AES (Ultima II, Horiba Jobin-Yvon, Edison, NJ, USA) to indicate the cellulose surface sulfation or charge (Chen et al., 2015), and the final CNCs have 0.94 wt% sulfur in sodium form.

ACS grade NaOH (99.5%), KOH (99.5%), K_2CO_3 (99%), hexane, and methanol (MeOH, 99.8%) were all purchased from Fisher Scientific Co. (Pittsburgh, PA, USA). All chemicals were directly used as received without purification.

2.2. Preparation of canola oil fatty acid methyl ester (CME)

Commercial canola oil (sold under the name "Nature's Secret") was purchased from a local Costco warehouse (Middleton, WI). Canola oil fatty acid methyl ester of (CME) was synthesized by a modified method described elsewhere (Lang et al., 2001). The reaction was conducted under excess methanol (MeOH) with molar ratio of MeOH to oil of 6:1. Catalyst (NaOH) concentration was 1 wt% of the oil and methanol mixture. The NaOH pellets were placed in MeOH and stirred with magnetic stirrer bar until completely dissolved. This mixture (66 g) was quickly added to oil (150 g) in a round bottom flask (500 mL) and stirred for 2 h at 70 °C. The reaction was conducted using a reflux apparatus with a condenser was used. After the reaction was complete, crude glycerol was separated in a separatory funnel. The top ester layer was dissolved in KOH (0.5 wt% of the mixture) solution of MeOH for the second reaction for 2 h at 25 °C to ensure full conversion to CME. The crude CME was separated and washed with hot water (70 °C) until the liquid was transparent and neutral pH. Traces of non-reacted MeOH were removed by purging with N_2 for 12 h.

2.3. Canola oil fatty acid methyl ester composition by GC–MS

The CME (2.0 mg) was weighed into a GC vial to which 2 mL of CH_2Cl_2 was added. CH_2Cl_2 contained 1-napthalaneacetic acid methyl ester as an internal standard (50 μg/mL). The as-prepared samples were analyzed using a Varian (Walnut Creek, CA, USA) model 3800 gas chromatograph interfaced to a Varian model 4000 ion trap mass detector, operated in full scan EI mode at 70 eV in the range m/z = 80–600. The transfer line was maintained at 250 °C. A Restek (Bellefonte, PA) Rxi-1MS column (30 m, 0.25 mm ID, 0.25 μm thickness) was temperature programmed 40 °C for 1 min, and then ramped at 5 °C/min to 290 °C for 2 min. A CombiPal auto-sampler (CTC Analytics, Zwingen, Switzerland) equipped with a 10 μL liquid syringe was used for 1 μL injections made in split mode 50:1, with injection port temperature of 200 °C. Helium (99.9999%) was used as carrier gas at a flow of 1 mL/min.

2.4. Transesterification of CNCs

Catalyst (K_2CO_3, 0.2 wt% of the total dry weight of CME and CNCs) was dissolved in MeOH first with constant stirring for 30 min, after which the excessive amount of CME (220 g) and CNC (10 g) powders were added (Note: the non-reacted CME can be recycled and reused to avoid waste). The reactant mixture was heated to 90 °C to drive off the MeOH to form a foaming soap. The remaining MeOH was further removed by applying intermittent vacuum to the flask until foaming subsided. A condenser installed to the flask and vacuum (10 mbar) applied and the mixture was heated to temperature (T_R = 100 and 120 °C) for a defined period of reaction time (t_R = 4, 8, 14, 20, and 30 h). The CNC fatty acid ester (CNCFE) was recovered by filtration then Soxhlet extracted with hexane for 12 h to remove non-reacted CME. The CNCFE was dried under vacuum overnight and weighed to determine the weight percentage gain (WPG%).

$$\mathrm{WPG\%} = (W_{CNCFE} - W_{CNC})/W_{CNC} \times 100 \quad (1)$$

where W_{CNCFE} is the dry weight of hexane extracted CNCFE after transesterification, while W_{CNC} is the weight of CNC before the reaction. The reaction time (t_R) and temperature (T_R) were attempted to tune the WPG%. The reaction mechanism is shown in Fig. 1.

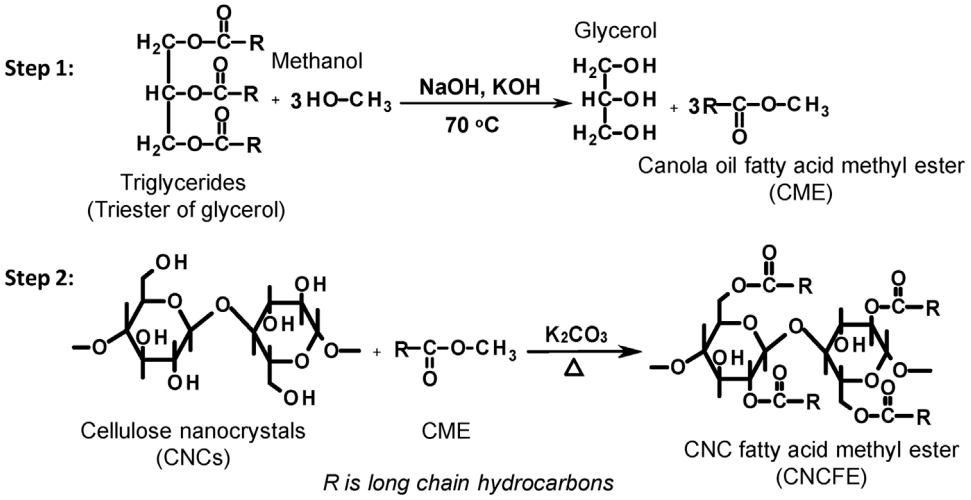

Fig. 1. Reaction mechanism illustration for the synthesis of CME (Step 1) and CNCFE (Step 2).

The number of OH groups substituted in CNCs after transesterification were estimated based on WPG and the molecular weight of the adduct with an assumption of 1:1 molar reaction between CME and CNC hydroxyl groups (Wei, McDonald, Freitag, & Morrell, 2013). The equation used to account for the hydrogen atom transferred from CNC to MeOH (1 in the equation) is shown as follows:

$$\text{OH substituted (mmol/g dry CNCs)} = 0.01 \times \text{WPG}/(\text{Molecular weight of adduct} - 1) \times 1000 \quad (2)$$

where the molecular weight of adduct was estimated from gas chromatography mass spectrometry (GC–MS) analysis of CME samples.

2.5. Surface chemistry of CNCs by FT-IR and FT-Raman spectroscopes

Unmodified CNCs and CNCFE samples were characterized by FT-IR spectroscopy using a Thermo Nicolet iZ10 FTIR spectrometer (attenuated total reflection (ATR) probe, Thermo Scientific, Verona, Wisconsin) using a smart iTR Basic accessory. A diamond crystal with 45° incident angle was used. The absorbance spectra were taken for an average of 128 scans in the range of 4000–600 cm^{-1} with the resolution of 4 cm^{-1}. Samples (in triplicates) were analyzed after vacuum drying. The spectra were baseline corrected, averaged, and normalized to the band at 1031 cm^{-1} using software Omnic v9.0 (Thermo Scientific).

Chemical and crystalline structures of unmodified CNC and CNCFE samples were analyzed by Raman spectroscopy with a Bruker MultiRam spectrometer (Bruker Instruments Inc., Billerica, Massachusetts) equipped with a 1064 nm 1000 mW continuous-wave (CW) diode pumped Nd:YAG laser. Approximately 200 mg of each sample was pressed into a pellet. The laser power used for sample excitation was 600 mW per sample spectrum and 1024 scans were accumulated. The Raman spectra were processed by the Bruker's OPUS software and normalized to the band at 1096 cm^{-1}.

2.6. Thermostability of nanocrystals

Thermogravimetric analysis (TGA) of CME, unmodified CNC, and CNCFE was conducted on a PerkinElmer Pyris 1 analyzer at a heating rate of 20 °C/min under N_2 atmosphere (20 mL/min).

2.7. Morphology

Transmission electron microscope (TEM) was used to study the morphology of unmodified CNCs before freeze-drying process. CNC suspension was diluted with distilled water and sonicated to disperse the CNC particles, and then an aliquot was deposited on a glow-discharged copper grid with formvar and carbon film (400 mesh). The grid was floated on drops of approximately 5 μL sample for 2 min, and then rinsed with two consecutive 250 μL drops of 2% aqueous uranyl acetate. Excess stain was removed by capillary action by gentle blotting. The samples were imaged using a Philips CM100 TEM (Philips/FEI, Eindhoven, The Netherlands) operated at 100 kV, spot 3200 μm condenser aperture, and 70 μm objective aperture. The images were captured and recorded using a SIA L3C 4-2 M pixel CCD camera (Scientific Instruments and Application, Duluth, GA).

Freeze-dried unmodified CNCs and transesterified CNCs power were directly deposited onto carbon tape. All samples were coated with a thin layer of gold. The prepared samples were investigated using a LEO Gemini field emission scanning electron microscope (SEM) operated at 3 kV under high vacuum.

2.8. Crystalline structure by wide angle X-ray diffraction (XRD) and FT-Raman

The crystalline structures of unmodified CNCs and CNCFE were characterized by wide angle X-ray diffraction spectroscopy (D8 Discover diffractometer, Bruker AXS Inc., WI, USA). The instrument was set up with a rotating Cu Kα2 X-ray IMS tube operating at 50 kV and 1000 μA. Scanning was performed over 2θ ranging from 5 to 60° with steps of 0.005°. The collected diffractograms were processed and peaks of interest were fitted (Gaussian function) using IGOR Pro v6 software. The intensity of each peak identified by peak fitting was mathematically computed. The approaches to calculate the crystallinity index of nanocrystals (CNC and CNCFE) and PLA are given as follows (Segal, Creely, Martin, & Conrad, 1959):

$$\text{CrI\%}_{\text{CNC/CNCFE}} = (1 - (I_{am}/I_{002})) \times 100 \quad (3)$$

where I_{am} is the intensity of amorphous diffraction, which is taken at 2θ angle between (002) and (101) peaks where the intensity is at minimum, and I_{002} is the maximum intensity of the (002) plane diffraction.

The crystal size dimension (D_{hkl}) was estimated by Scherrer's formula: (Alexander, 1969)

$$D_{hkl} = K \times \lambda / (\beta_{1/2} \times \cos\theta) \quad (4)$$

where K is the crystal shape constant taken to be 0.9, λ is the X-ray wavelength (λ = 0.1542 nm), $\beta_{1/2}$ is the angular full width half maximum (FWHM) of the interested peak in radians obtained by IGOR Pro software when peak fitting was conducted with the Gaussian function, and θ is the diffraction angle in radians.

The spacing between the (002) planes, d, was calculate using the Bragg's equation:

$$n\lambda = 2d\sin\theta \quad (5)$$

where n is an integer, λ is the wavelength of the incident wave, and θ is the angle between the incident ray and the scattering planes.

Crystallinities by FT-Raman were estimated using the 380-Raman method (Agarwal, Ralph, & Reiner, 2013; Agarwal, Reiner, & Ralph, 2010) and are based on the following equations.

$$X_{MultiRam} = ((I_{380}/I_{1,096}) - 0.0286)/0.0065 \quad (6)$$

$$X_{RFS\text{-}100} = (X_{MultiRam} + 2.0212)/0.8222 \quad (7)$$

where I_{380} and I_{1096} stands for the intensity of peaks at 380 cm^{-1} and 1096 cm^{-1} for Raman spectra collected by the Raman instrument, MultiRam, while $X_{RFS\text{-}100}$ and $X_{MultiRam}$ represent the crystallinity values obtained from Raman spectra collected by using two Raman instruments, the RFS-100 and MultiRam, respectively.

2.9. Water contact angle measurements

The surface hydrophilicity of unmodified and transesterified CNCs was evaluated by contact angle measurements using a KSV Attension Theta Lite Optical Tensiometer. CNC/CNCFE powder was compression molded into discs (12 mm Ø × 1.5 mm) at 20 MPa using a hydraulic press (Carver). The static contact angle between a water droplet (10 μL) and the CNC disc was measured. The contact angle was recorded from the captured images at from 0 to 10 s.

3. Results and discussion

3.1. CME composition

A total of five different fatty acids were identified in CME, as shown in Table 1. The dominant fatty acid in canola oil was oleic acid (C18:1) at 66.6%, followed by linoleic acid (C18:2) (23.8%), linolenic acid (C18:3) (6.8%), palmitic acid (C16:0) (1.8%), and stearic acid (C18:0) (1.0%). This result agrees well to previous reports (Lang et al., 2001). It is worth noting that the chemical nature of CME obtained in this study is FAME which is the constituent of biodiesel. Hence, the CME to be used to modify CNCs, which will be discussed later, can be substituted by commercial biodiesel with higher purity. The approximate M_w of the CME mixture is 294.5 g/mol, which is close to the value of 297.1 g/mol that was reported elsewhere (He, Singh, & Thompson, 2005).

3.2. Chemical structure changes of nanocrystals

In order to maximize the conversion of CNC into CNCFE via transesterification (Fig. 1), excess amount of CME was used in the reaction (molar ratio of CNCs to CME = 1:12). The WPG% and the visual appearance of modified CNCs are dependent on the reaction conditions, reaction time (t_R) and reaction temperature (T_R) (Supplementary Table S1). When the same T_R (100 °C) was used the WPG% was increased from 5.5 to 10.0% and 10.5% with t_R was increased from 4 to 14 and 20 h, respectively. The WPG% was not increased any more with the t_R was increased from 20 to 30 h.

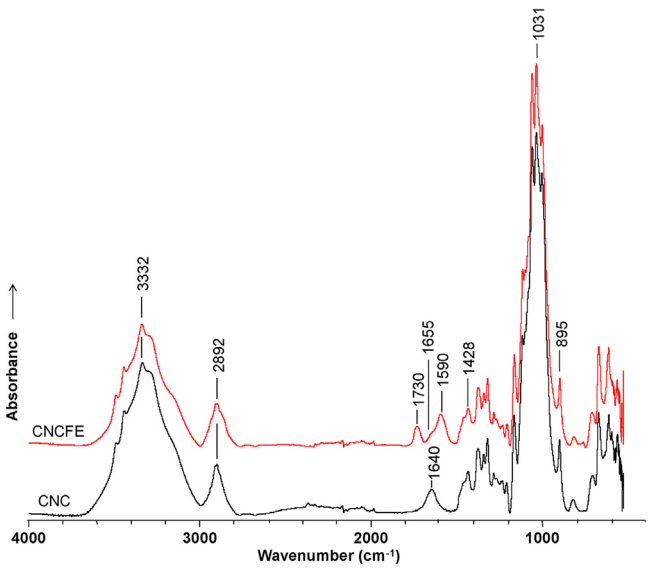

Fig. 2. FT-IR spectra of unmodified and transesterified CNCs.

Although higher T_R yields higher WPG%, the CNCFE showed discoloration/darkening when the reaction temperature was increased from 100 to 120 °C. This may be contributed to the degradation of sulfate groups on the CNCs, and relatively low thermal stability is a disadvantage of CNCs produced from conventional concentrated sulfuric acid hydrolysis (Chen, Zhu, Baez, Kitin, & Elder, 2016). By changing the t_R and T_R, WPG% and the OH groups substituted as well can be monitored. For example, when the t_R was optimized to be 20 h at T_R = 120 °C, giving an average WPG% (two batches) of transesterification was 12.5 ± 1.2%. The degree of OH groups substituted after transesterification was calculated from Eq. (2) based on WPG was 0.5 mmol/g dry CNC. CNCFE sample obtained under this reaction conditions was selected for further characterization. According to the final applications of the transesterified CNCs, by changing the reaction time and temperature the modification efficiency (OH substitution) and appearance can be tuned.

FT-IR spectra showed that esterification induced a number of chemical changes in the CNC (Fig. 2). Carbonyl groups were assigned to the aliphatic esters for CNCFE at 1730 cm^{-1} (Wei et al., 2013). This provides evidence that transesterification was successful. The degree of transesterification (D_1) was estimated from the ratio of I_{1730}/I_{1031} to be 0.1, where I_{1730} and I_{1031} are the intensity of the C=O stretching band and the C—O stretching of cellulose backbone at about 1730 cm^{-1} and 1031 cm^{-1}, respectively. It is worth noting that the D_1 value was lower than the degree of acetylation of CNC by vinyl acetate reported by Ramírez et al., which used citric acid as catalyst (Ramírez et al., 2016). The band for CNCs at 1640 cm^{-1} is ascribed to the absorbed water (H—O—H) which was absent in CNCFE (Jabbari, Wisniewski, & Peppas, 1993). A new band at 1590 cm^{-1} was observed in the spectrum of CNCFE which is assigned to C=C stretching within the hydrocarbon chain of unsaturated fatty acid fragments such as C18:1, C18:2, and C18:3 (Mayo, Miller, & Hannah, 2003). In addition, no peak (or even a shoulder) was observed at 2853 cm^{-1} (—O—CH_3 stretch), indicating the CME was removed completely by hexane extraction. This further supported that the transesterification was successful.

3.3. Structural and crystallinity changes of cellulose I

The surface chemistry of transesterified CNCs was further characterized by Raman. The spectra of unmodified CNC and CNCFE are shown in Fig. 3. The band of CNCFE at 1655 cm^{-1} was assigned to C=C stretching of the hydrocarbon chain of C18:1, C18:2 and C18:3.

Table 1
Chemical composition profiles of CME determined by GC–MS.

Compounds	Retention time (min)	M^+ (*m/z*)	Relative concentration (%)
Methyl palmitate (C16:0)	10.59	270	1.8
Methyl linolenate (C18:3)	21.47	292	6.8
Methyl linoleoate (C18:2)	21.11	294	23.8
Methyl oleioate (C18:1)	21.93	296	66.6
Methyl stearate (C18:0)	24.65	298	1.0

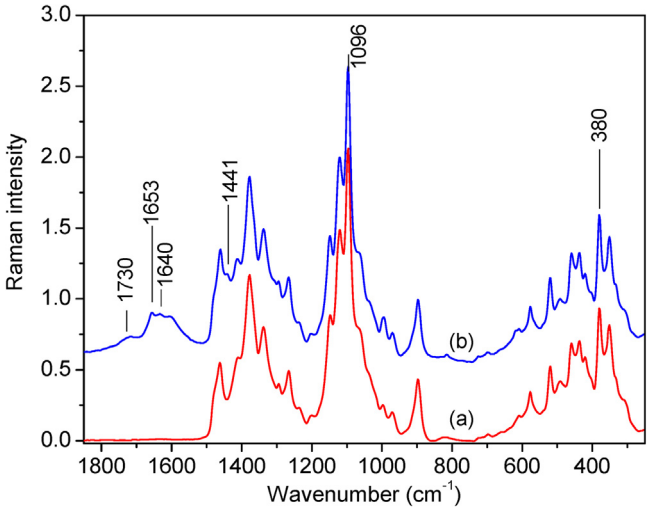

Fig. 3. Raman spectra in the region of 1850–250 cm^{-1} of (a) CNC and (b) CNCFE.

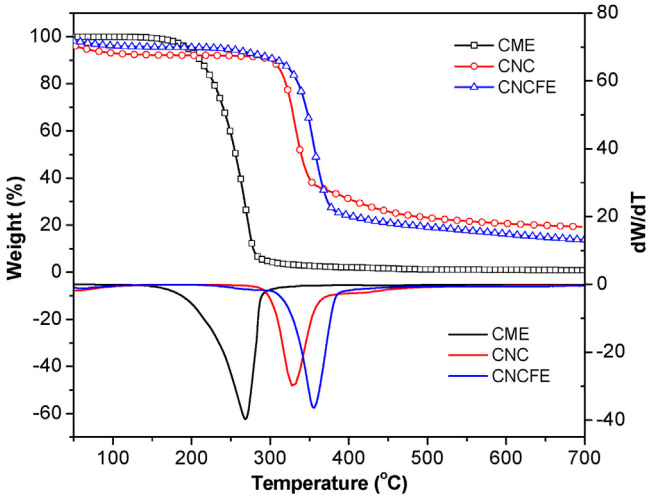

Fig. 4. TG and DTG curves of CME, CNC, and CNCFE.

This is consistent with the FTIR results. The weak ester C=O stretching band appears at 1720 cm^{-1}. According to the method developed by Agarwal et al. (Agarwal, Ralph et al., 2013; Agarwal, Ralph, Reiner, & Baez, 2015; Agarwal et al., 2010), FT-Raman spectroscopy was used to characterize the crystalline structure of cellulose I. The extent of cellulose I crystallinity was determined by the intensity ratio of the 380 and 1096 cm^{-1} bands from the Raman spectra, which was 43% and 47% for unmodified CNC and CNCFE samples, respectively. This crystallinity was lower than values that were reported previously for CNCs, i.e., 54–66% (Agarwal, Reiner, & Ralph, 2013; Chen et al., 2015), likely because there is a significant amount of cellulose II in the CNCs produced from dissolving pulp obtained by alkaline pulping and acid hydrolysis processes. Also, noteworthy is the fact that even for all cellulose I CNCs 380-Raman crystallinities are usually significantly lower compared to XRD methods (Agarwal, Reiner et al., 2013; Chen et al., 2015). Crystallinity of cellulose I was not significantly changed, suggesting its crystal network wasn't interrupted by transesterification. Since the high degree of crystallinity of CNC is one of the major reasons given for its attractive mechanical, physical and chemical properties (Habibi et al., 2010; Moon et al., 2013), it is expected that the mechanical strength is maintained after modification with CME to form CNCFE.

3.4. Thermal stability of nanocrystals

The thermal stability of CNCFE was found to be higher than CME and unmodified CNCs as shown in thermogravimetric (TG) and derivative thermogravimetric (DTG) curves (Fig. 4). The mass loss due to thermal degradation of CME occurred in one stage with the onset degradation temperature (T_{onset}) of 168 °C. During this stage CME was completely decomposed at T_{com} = 307 °C. About 60 wt% of unmodified CNC sample was degraded at T ≤ 350 °C followed by the second stage (350–450 °C) caused by the depolymerization and decomposition of cellulose glycosyl units (Shen, Gu, & Bridgwater, 2010; Wei, McDonald, & Stark, 2015). The char residual yield of unmodified CNC at 600 °C was about 21 wt%. The temperature of maximum decomposition rate (T_{max}) in CNCFE was 28 °C higher than that of unmodified CNC (327 °C), while the residual at the end was about 16 wt%. We conclude, therefore, that transesterification improved the thermal stability of CNC with CME, even though CME itself is less thermally stable. The improved thermal stability of transesterified nanocrystals could broaden the melt processing window when being compounded with polymer for nanocomposites.

3.5. Surface morphological studies

The TEM image in Fig. 5a shows the structure and dimension of CNCs produced from dissolving pulp. It can be seen that CNCs have rod-like shape and were separated without aggregation before the freeze-drying process. Size measurements were made using an image analysis software Fiji (http://imagej.net/Fiji). The CNCs had a broad size distribution, with the length and diameter ranges of 25–150 nm and 5–18 nm, respectively, and averages of 78 ± 30 nm and 11 ± 2 nm, respectively. The CNCs derived from sulfuric acid hydrolysis always have smaller dimensions than those produced by other approaches (Chen et al., 2015; Klemm et al., 2011).

SEM micrographs of unmodified CNC and CNCFE surfaces are shown in Fig. 5b–d. The unmodified CNC suspension (10.7 wt%) was directly deposited onto carbon tape and dried under air before SEM examination. As shown in Fig. 5b, the air-dried CNCs are lamella/sheet like flakes. The freeze-dried unmodified CNCs (Fig. 5c) lost the rod-like shape morphology as well. The presence of micro-scale agglomerated CNCs with larger sizes than air-dried CNCs, as shown in Fig. 5c, are possibly originated from the hydrogen-bonding and van der Waals forces during freeze-drying of the CNC suspension (10.7 wt%). Micro-scaled aggregates were found by researches previously (Fumagalli, Sanchez, Boisseau, & Heux, 2013; Han, Zhou, Wu, Liu, & Wu, 2013). Agglomerates sizes become smaller after transesterification. Moreover, the surface structure of CNCFE agglomerated flakes seems to be rougher

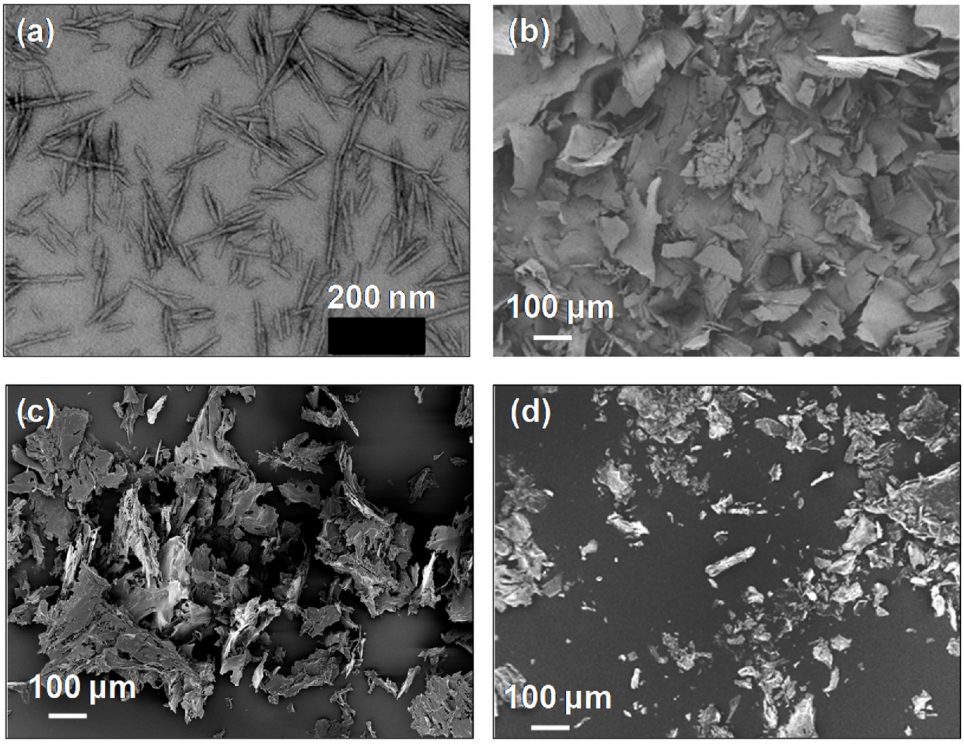

Fig. 5. Transmission electron micrograph of CNCs (a) and scanning electron micrographs of unmodified CNC suspension (10.7 wt%) (b), freeze-dried unmodified CNCs (c) and CNCFE (d).

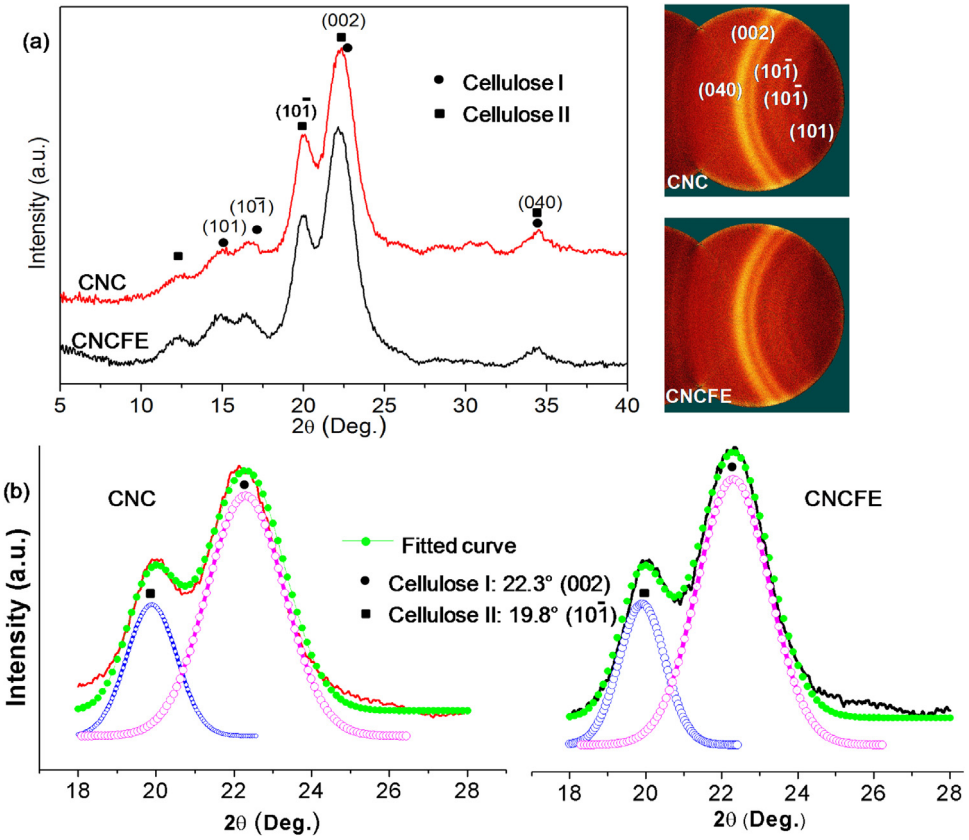

Fig. 6. XRD diffractograms and patterns (a) and fitted peaks for cellulose I and cellulose II (b) of unmodified CNC and CNCFE.

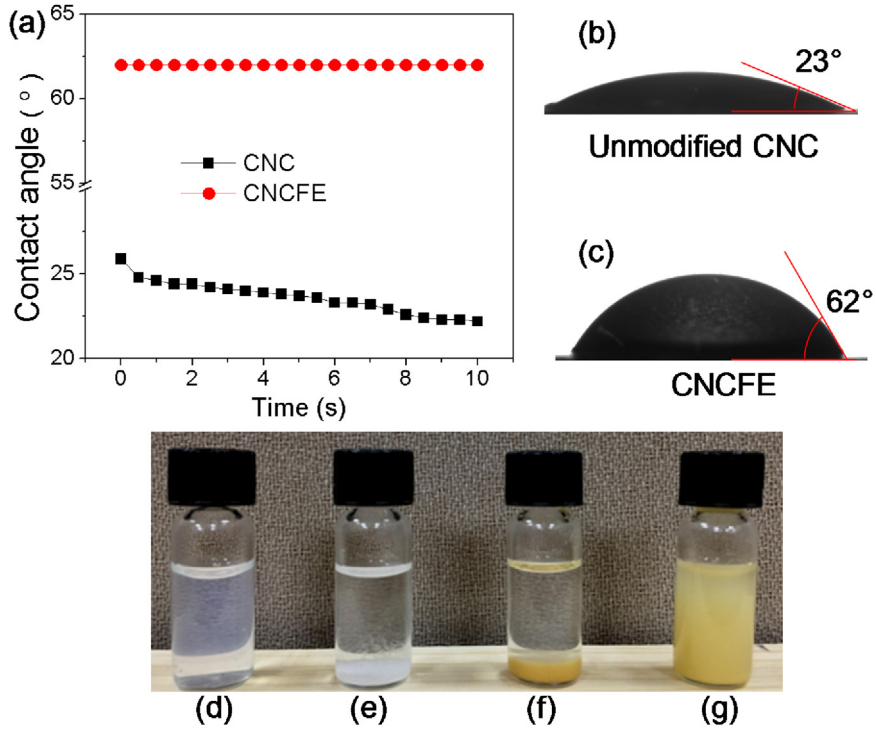

Fig. 7. Dynamic water contact angles versus time (a), water contact angles measured on surfaces of unmodified CNCs (b) and CNCFE (c) after 5 s, and suspensions of unmodified CNCs in water (d) and hexane (e), and the CNCFE in water (f) and hexane (g).

Table 2
XRD results of unmodified CNC and CNCFE.[a]

	2θ	FWHM (°)	d (Å)	D_{002} (Å)	$D_{10\bar{1}}$ (Å)	$CrI\%_{CNC/CNCFE}$	Cell-I/Cell-II
CNC	20.0	1.165	8.9		69		
	22.3	1.832	7.9	44		76.9	1.98
CNCFE	20.0	1.166	8.9		69		
	22.3	1.748	7.9	44		75.1	

[a] Crystal sizes were determined in the direction perpendicular to the planes of (002) of cellulose I and ($10\bar{1}$) of cellulose II, respectively.

(Fig. 5d), which is likely caused by the mechanically shearing/washing during the transesterification reaction.

3.6. Crystalline structure

The effect of transesterification on the crystalline structure of unmodified CNC and CNCFE was investigated by XRD analysis. The diffraction patterns are shown in Fig. 6. Unmodified CNCs showed diffraction peaks at 14.5°, 16.5°, 22.3°, and 34.5°, being assigned to cellulose I crystal planes (101), ($10\bar{1}$), (002), and (040), respectively (Zuluaga et al., 2009). Diffractions from cellulose II are also present in unmodified CNCs at 2θ of 12.5°, 19.8° ($10\bar{1}$), 21.9°, and 34.5°. Cellulose I can be transformed to cellulose II during alkali pulping and acid hydrolysis process originated from dissolving pulp preparation stage (El Oudiani, Chaabouni, Msahli, & Sakli, 2011). The ratio of peak intensity at 22.3° vs. intensity at 19.8° ($I_{22.3°}/I_{19.8°}$) is used to estimate the Cellulose I vs. cellulose II content (Gindl & Keckes, 2005). The peak intensities were obtained by peak fitting of XRD diffractograms (Fig. 6b). $I_{22.3°}/I_{19.8°}$ of CNC and CNCFE was 2.00 and 1.98, respectively, indicating the CNC crystalline structure was not influenced by this transesterification modification. Diffraction patterns of CNCFE are similar to those of unmodified CNCs sample, suggesting transesterification did not change crystalline structure of the nanocrystals. This was further supported by Raman spectroscopy (Fig. 3) where intensity of bands that were associated with the crystalline structures was similar between unmodified CNCs and CNCFE.

The results obtained from fitted peaks of peak angle (2θ), FWHM, average crystal size (D_{hkl}) in the direction perpendicular to the reflection plane, and crystallinity indices ($CrI\%_{CNC/CNCFE}$) are listed in Table 2. The crystallinity indices were 76.9% for unmodified CNCs and 75.1% for CNCFE, while the crystallinity of original wood pulp was about 76% (Chen et al., 2015). Hence, crystallinity index of cellulose was not altered during transformation of wood pulp to CNCs. The average crystal width for cellulose I and cellulose II were 44 Å (D_{002}) and 69 Å ($D_{10\bar{1}}$) respectively, for both unmodified and CNCFE. These values are consistent with reported values of cellulose I and II nanocrystals (Sèbe, Ham-Pichavant, Ibarboure, Koffi, & Tingaut, 2012). It is therefore concluded that neither the crystal size nor the degree of crystallinity of CNCs were affected by transesterification, and hence, crystal mechanical strength was expected to be retained. This is consistent with the cellulose I crystallinity results from quantitative Raman spectroscopic analysis discussed above.

3.7. Hydrophobicity changes

The water contact angle results are given in Fig. 7. The dynamic contact angle changes with time (0–10 s) showed that the CNCFE surface is significantly more hydrophobic, as indicated by higher contact values of CNCFE (62°) than the unmodified CNCs (23°) (Fig. 7a–c). The relatively lower contact angles were obtained

as compared with acetylated CNC films as reported previously, which could be contributed to the lower degree of OH substituted (Abraham et al., 2016). The unmodified CNC surface showed water droplet spreading with time as compared to the CNCFE. Photographs of suspensions of freeze-dried unmodified CNCs and the CNCFE re-dispersed in water/hexane (Fig. 7d–g). The suspension was treated with sonication for 10 min at 50% of maximum power using a tip-type Ultrasonic processor (Sonisc Vibracell, ThermoFisher, USA), and then allowed for 30 min before photographs were taken. The re-dispersed freeze-dried unmodified CNCs formed a homogeneous and stable suspension in water but settled in hexane, while the CNCFE settled in water but formed a stable suspension in hexane. This confirmed further that the significantly increased hydrophobicity of tranesterified CNC increased its dispersion ability in hexane, a non-polar solvent.

4. Conclusions

Cellulose nanocrystals were successfully transesterified with a sustainable and green chemistry-based approach using vegetable oil fatty acid methyl ester. This functionalization method on cellulose nanomaterials is reported here for the first time. The degree of crystallinity and crystalline structure of nanocrystals were not altered by functionalization. The transesterified CNC showed improved thermal stability as compared to unmodified CNC. The particle sizes of transesterified CNC agglomerates were smaller than unmodified equivalents. The transesterified CNC surfaces are significantly more hydrophobic than the unmodified CNCs. This transesterification strategy has the potential to be employed to modify other cellulose nanomaterials, i.e. CNF, having higher availability of OH groups on surface. The byproduct, crude glycerol, during the CME production process can be recycled and potentially used as emulsions and polymer processing aids for future research. This research could broaden the application of cellulose nanomaterials in the fields of coatings, emulsions, and nanocomposites, and therefore facilitate its commercialization.

Acknowledgements

The authors thank the funding from Public-Private Partnership for Nanotechnology (P^3Nano) US Endowment for Forestry and Communities, Inc. (Grant No. CWFSCL15). We also acknowledge the following people from the USDA Forest Service, Forest Products Laboratory: Richard S. Reiner for preparing CNCs, Dr. Craig Clemons and Philip Walsh for help with TGA, Dr. J.Y. Zhu and Huiyang Bian for water contact angle measurements, and Sally A. Ralph for Raman experiments.

Appendix A. Supplementary data

Supplementary data associated with this article can be found, in the online version, at http://dx.doi.org/10.1016/j.carbpol.2017.04.008.

References

Abraham, E., Kam, D., Nevo, Y., Slattegard, R., Rivkin, A., Lapidot, S., & Shoseyov, O. (2016). Highly modified cellulose nanocrystals and formation of epoxy-nanocrystalline cellulose (CNC) nanocomposites. *ACS Applied Materials & Interfaces*, *8*(41), 28086–28095.

Agarwal, U. P., Reiner, R. S., & Ralph, S. A. (2010). Cellulose I crystallinity determination using FT–Raman spectroscopy: Univariate and multivariate methods. *Cellulose*, *17*(4), 721–733.

Agarwal, U. P., Ralph, S. A., Reiner, R. S., & Baez, C. (2015). Probing crystallinity of never-dried wood cellulose with Raman spectroscopy. *Cellulose*, *23*(1), 125–144.

Agarwal, U. P., Ralph, S. A., & Reiner, R. S. (2013). Estimation of cellulose crystallinity of lignocelluloses using near-IR FT-Raman Spectroscopy and comparison of the Raman and Segal-WAXS methods. *Journal of Agricultural and Food Chemistry*, *61*(1), 103–113.

Agarwal, U. P., Reiner, R. S., & Ralph, S. A. (2013). Crystallinity of nanocellulose materials by near-IR FT-Raman spectroscopy. In M. T. Postek, R. J. Moon, A. W. Rudie, & M. A. Bilodeau (Eds.), *Production and applications of cellulose nanomaterials* (pp. 43–44). Peachtree Corners, GA: TAPPI Press.

Alexander, L. E. (1969). *X-ray diffraction method in polymer science*. New York, USA: Wiley-Interscience.

Bardet, R., Roussel, F., Coindeau, S., Belgacem, N., & Bras, J. (2015). Engineered pigments based on iridescent cellulose nanocrystal films. *Carbohydrate Polymers*, *122*, 367–375.

Boujemaoui, A., Mongkhontreerat, S., Malmström, E., & Carlmark, A. (2015). Preparation and characterization of functionalized cellulose nanocrystals. *Carbohydrate Polymers*, *115*, 457–464.

Chen, L., Wang, Q., Hirth, K., Baez, C., Agarwal, U. P., & Zhu, J. Y. (2015). Tailoring the yield and characteristics of wood cellulose nanocrystals (CNC) using concentrated acid hydrolysis. *Cellulose*, *22*(3), 1753–1762.

Chen, L., Zhu, J. Y., Baez, C., Kitin, P., & Elder, T. (2016). Highly thermal-stable and functional cellulose nanocrystals and nanofibrils produced using fully recyclable organic acids. *Green Chemistry*, *18*(13), 3835–3843.

El Oudiani, A., Chaabouni, Y., Msahli, S., & Sakli, F. (2011). Crystal transition from cellulose I to cellulose II in NaOH treated Agave americana L. fibre. *Carbohydrate Polymers*, *86*(3), 1221–1229.

Espino-Pérez, E., Domenek, S., Belgacem, N., Sillard, C., & Bras, J. (2014). Green process for chemical functionalization of nanocellulose with carboxylic acids. *Biomacromolecules*, *15*(12), 4551–4560.

Eyley, S., & Thielemans, W. (2011). Imidazolium grafted cellulose nanocrystals for ion exchange applications. *Chemical Communications*, *47*(14), 4177.

Fumagalli, M., Sanchez, F., Boisseau, S. M., & Heux, L. (2013). Gas-phase esterification of cellulose nanocrystal aerogels for colloidal dispersion in apolar solvents. *Soft Matter*, *9*(47), 11309–11317.

Gindl, W., & Keckes, J. (2005). All-cellulose nanocomposite. *Polymer*, *46*(23), 10221–10225.

Habibi, Y., Lucia, L. A., & Rojas, O. J. (2010). Cellulose nanocrystals: Chemistry self-assembly, and applications. *Chemical Reviews*, *110*, 3479–3500.

Han, J., Zhou, C., Wu, Y., Liu, F., & Wu, Q. (2013). Self-assembling behavior of cellulose nanoparticles during freeze-drying: Effect of suspension concentration, particle size, crystal structure, and surface charge. *Biomacromolecules*, *14*(5), 1529–1540.

Hatton, F. L., Kedzior, S. A., Cranston, E. D., & Carlmark, A. (2017). Grafting-from cellulose nanocrystals via photoinduced Cu-mediated reversible-deactivation radical polymerization. *Carbohydrate Polymers*, *157*, 1033–1040.

He, B. B., Singh, A. P., & Thompson, J. C. (2005). Experimental optimization of a continuous-flow reactive distillation reactor for biodiesel production. *Transactions of the ASAE*, *48*(6), 2237–2243.

Jabbari, E., Wisniewski, N., & Peppas, N. A. (1993). Evidence of mucoadhesion by chain interpenetration at a poly (acrylic acid)/mucin interface using ATR-FTIR spectroscopy. *Journal of Controlled Release*, *26*(2), 99–108.

Klemm, D., Heublein, B., Fink, H.-P., & Bohn, A. (2005). Cellulose: Fascinating biopolymer and sustainable raw material. *Angewandte Chemie International Edition*, *44*(22), 3358–3393.

Klemm, D., Kramer, F., Moritz, S., Lindström, T., Ankerfors, M., Gray, D., & Dorris, A. (2011). Nanocelluloses: A new family of nature-based materials. *Angewandte Chemie International Edition*, *50*(24), 5438–5466.

Lang, X., Dalai, A. K., Bakhshi, N. N., Reaney, M. J., & Hertz, P. B. (2001). Preparation and characterization of bio-diesels from various bio-oils. *Bioresource Technology*, *80*(1), 53–62.

Lin, N., Huang, J., Chang, P. R., Feng, J., & Yu, J. (2011). Surface acetylation of cellulose nanocrystal and its reinforcing function in poly(lactic acid). *Carbohydrate Polymers*, *83*(4), 1834–1842.

Mayo, D. W., Miller, F. A., & Hannah, R. W. (2003). *Course notes on the interpretation of infrared and Raman spectra*. Hoboken, New Jersey: John Wiley & Sons, Inc.

Moon, R. J., Beck, S., & Rudie, A. W. (2013). Cellulose nanocrystals—A material with unique properties and many potential applications. In M. T. Postek, R. J. Moon, A. W. Rudie, & M. A. Bilodeau (Eds.), *Production and applications of cellulose nanomaterials* (pp. 9–12). Peachtree Corners, GA: TAPPI Press.

Morandi, G., Heath, L., & Thielemans, W. (2009). Cellulose Nanocrystals grafted with polystyrene chains through surface-initiated atom transfer radical polymerization (SI-ATRP). *Langmuir*, *25*(14), 8280–8286.

Pereira, A. L. S., Nascimento, D. M. D., Souza Filho, M. D. S. M., Morais, J. P. S., Vasconcelos, N. F., Feitosa, J. P. A., . . . & Rosa, M. D. F. (2014). Improvement of polyvinyl alcohol properties by adding nanocrystalline cellulose isolated from banana pseudostems. *Carbohydrate Polymers*, *112*, 165–172.

Ramírez, J. A. A., Fortunati, E., Kenny, J. M., Torre, L., & Foresti, M. L. (2016). Simple citric acid-catalyzed surface esterification of cellulose nanocrystals. *Carbohydrate Polymers*, *57*, 1358–1364.

Reiner, R., & Rudie, A. (2013). Process scale-up of cellulose nanocrystal production to 25 kg per batch at the forest products laboratory. In M. T. Postek, R. J. Moon, A. W. Rudie, & M. A. Bilodeau (Eds.), *Production and applications of cellulose nanomaterials* (pp. 21–24). Peachtree Corners, GA: TAPPI Press.

Sèbe, G., Ham-Pichavant, F., Ibarboure, E., Koffi, A. L. C., & Tingaut, P. (2012). Supramolecular structure characterization of cellulose II nanowhiskers produced by acid hydrolysis of cellulose I substrates. *Biomacromolecules*, *13*(2), 570–578.

Segal, L., Creely, J., Martin, A., Jr., & Conrad, C. (1959). An empirical method for estimating the degree of crystallinity of native cellulose using the X-ray diffractometer. *Textile Research Journal*, *29*(10), 786–794.

Shen, D. K., Gu, S., & Bridgwater, A. V. (2010). The thermal performance of the polysaccharides extracted from hardwood: Cellulose and hemicellulose. *Carbohydrate Polymers*, *82*(1), 39–45.

Wang, Q. Q., Zhu, J. Y., Reiner, R. S., Verrill, S. P., Baxa, U., & McNeil, S. E. (2012). Approaching zero cellulose loss in cellulose nanocrystal (CNC) production: Recovery and characterization of cellulosic solid residues (CSR) and CNC. *Cellulose*, *19*(6), 2033–2047.

Wei, L., & McDonald, A. (2016). A review on grafting of biofibers for biocomposites. *Materials*, *9*(4), 303, 310.3390/ma9040303

Wei, L., McDonald, A. G., Freitag, C., & Morrell, J. J. (2013). Effects of wood fiber esterification on properties, weatherability and biodurability of wood plastic composites. *Polymer Degradation and Stability*, *98*(7), 1348–1361.

Wei, L., McDonald, A. G., & Stark, N. M. (2015). Grafting of bacterial polyhydroxybutyrate (PHB) onto cellulose via in situ reactive extrusion with dicumyl peroxide. *Biomacromolecules*, *16*(3), 1040–1049.

Yoo, Y., & Youngblood, J. P. (2016). Green one-pot synthesis of surface hydrophobized cellulose nanocrystals in aqueous medium. *ACS Sustainable Chemistry & Engineering*, *4*(7), 3927–3938.

Zaman, M., Xiao, H., Chibante, F., & Ni, Y. (2012). Synthesis and characterization of cationically modified nanocrystalline cellulose. *Carbohydrate Polymers*, *89*(1), 163–170.

Zuluaga, R., Putaux, J. L., Cruz, J., Vélez, J., Mondragon, I., & Gañán, P. (2009). Cellulose microfibrils from banana rachis: Effect of alkaline treatments on structural and morphological features. *Carbohydrate Polymers*, *76*(1), 51–59.